SolarPACES 2024, 30th International Conference on Concentrating Solar Power, Thermal, and Chemical Energy Systems

Solar Fuels and Chemical Commodities

https://doi.org/10.52825/solarpaces.v3i.2429

© Authors. This work is licensed under a Creative Commons Attribution 4.0 International License

Published: 19 Nov. 2025

# Technoeconomic Analysis of a Solar Thermochemical Fuel Production Process Using a Packed-Bed Redox Reactor

Alon Lidor<sup>1,\*</sup> D, Zachary Hart<sup>1,2</sup>, and Janna Martinek<sup>1</sup>

<sup>1</sup>National Renewable Energy Laboratory, Colorado

<sup>2</sup>Pennsylvania State University, Pennsylvania

\*Correspondence: Alon Lidor, alon.lidor@nrel.gov

**Abstract.** The production of synthetic liquid fuels at a competitive price is paramount to deploy them at scale in sectors such as the aviation and maritime industries. Solar thermochemical fuel production is a promising pathway to produce such fuels using concentrated solar thermal (CST) driving high-temperature redox reactions, coupled with a gas-to-liquid process. In this work we present a preliminary technoeconomic analysis of a solar fuels plant, utilizing a new fixed-bed countercurrent redox reactor and combining both CST and photovoltaic arrays to supply the required energy. Three case studies are examined: CST-PV hybrid, CST-PV hybrid with energy conversion between heat and electricity, and CST. All cases include a power block that utilizes the exothermic heat of oxidation. A TEA framework, based on reduced order modelling of the redox reactor, is used to correlate design and operating conditions to syngas production rate. Preliminary analysis shows that commercial viability is unattainable for reduction temperatures up to 1500°C, attributable to the low feedstock conversion. When increasing the reduction temperature to 1600°C, levelized costs of hydrocarbon feedstock below \$10/gal are attainable. CST-PV hybrid with energy conversion is identified as the most promising configuration between the three configurations examined in this work. While calculated fuel costs are still much higher than those of fossil-based hydrocarbon fuels, several directions are identified that can improve their commercial viability, namely inclusion of thermal energy storage, increasing the overall plant scale, and further optimization of the CST and PV subsystems.

Keywords: Solar Fuels, Solar Thermochemical Fuel Production, System Modeling

#### 1. Introduction

Liquid hydrocarbon fuels are expected to remain a significant part of the future energy mix, due to their high specific energy (both gravimetric and volumetric), ease of storage and transport, and the large existing infrastructure. Some specific sectors which rely heavily on those fuels include aviation and maritime transportation. In order to reduce the dependence on fossil-based fuels, alternative synthetic fuels, produced at competitive costs, are needed. Synthetic liquid fuels can be generated by various gas-to-liquid (GTL) technologies such as Fischer-Tropsch, methanol (MeOH) synthesis, and others. However, these technologies require the use of synthetic gas (syngas) as the feedstock – a mixture of H<sub>2</sub> and CO at a specific ratio, depending on the exact process. The production of syngas using feedstocks such as CO<sub>2</sub> and H<sub>2</sub>O is the main challenge in the field of solar thermochemical fuel production. Different cycles and processes have been proposed to convert CO<sub>2</sub> and H<sub>2</sub>O into syngas, with the 2-step reduction-oxidation (redox) cycle being extensively pursued in the last 25 years. While

many reactor concepts and different materials have been proposed, only a handful of experimental demonstrations of note have been performed. To date, the most visible demonstrations are of a directly irradiated solar receiver-reactor in a volumetric cavity design, with  $CeO_2$  as the redox-active material. The highest reported reactor efficiency for syngas production was 4.1% in a volumetric cavity receiver with a thermal heat input of 50 kW [1], defined as the heating value of the products over the thermal heat input into the reactor (covering required sensible heating as well as the endothermic reduction enthalpy), vacuum pumping energy (to lower the  $O_2$  partial pressure), and inert gas separation energy. The two-step redox cycle chemical reactions are:

Reduction (endothermic): 
$$\frac{1}{\Delta\delta} CeO_{2-\delta_{\rm ox}} \rightarrow \frac{1}{\Delta\delta} CeO_{2-\delta_{\rm red}} + \frac{1}{2}O_2$$
 (1)

Oxidation with CO<sub>2</sub> (exothermic): 
$$\frac{1}{\Delta\delta} \text{CeO}_{2-\delta_{\text{red}}} + \text{CO}_2 \rightarrow \frac{1}{\Delta\delta} \text{CeO}_{2-\delta_{\text{ox}}} + \text{CO}$$
 (2)

Oxidation with H<sub>2</sub>O (exothermic): 
$$\frac{1}{\Lambda\delta} \text{CeO}_{2-\delta_{\text{red}}} + \text{H}_2\text{O} \rightarrow \frac{1}{\Lambda\delta} \text{CeO}_{2-\delta_{\text{ox}}} + \text{H}_2$$
 (3)

with  $\Delta\delta=\delta_{red}-\delta_{ox}$  as the difference in nonstoichiometry between reduction and oxidation.

Other important metrics, which affect the overall cycle performance and its scaling and economic potential, are usually overlooked in the field [2]. These include the feedstock conversion X, defined as the fraction of feedstock fed into the reactor that undergoes chemical conversion; the power output  $P_{\rm out}$ , defined as the rate of fuel production times the fuel heating value; and the power density  $P_{\rm out}/V$ , defined as the power output per unit volume or mass. When calculating these metrics for the aforementioned demonstration, one obtains values of  $X_{\rm H_2O} = 0.05$ ,  $X_{\rm CO_2} = 0.1$ ,  $P_{\rm out} = 304$  W, and  $P_{\rm out}/V = 6.9$  kW m<sup>-3</sup> (when considering only the cavity and redox-active material volumes, without the volume of the insulation, shell, and auxiliary systems). For comparison, a Bosch proton exchange membrane (PEM) electrolyzer unit has a value of  $\frac{P_{\rm out}}{V} = 785$  kW m<sup>-3</sup> (including the entire stack volume).

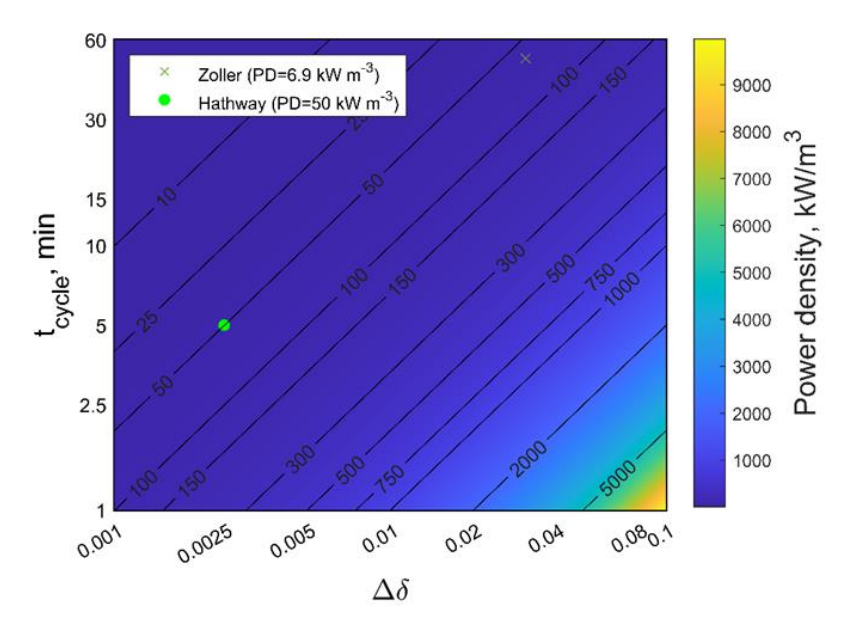


**Figure 1.** Power density as a function of the nonstoichiometry extent  $\Delta \delta$  and the cycle duration  $t_{cycle}$  for CeO<sub>2</sub>. Two values from published experimental work are included: a 50 kW<sub>th</sub> input volumetric receiver-reactor (Zoller et al. [1]) and a 4.4 kW<sub>th</sub> input packed bed reactor (Hathaway et al. [3]).

Increasing the reactor efficiency is not directly correlated with increasing the values of X,  $P_{\rm out}$ , and  $P_{\rm out}/V$ ; on the contrary, many strategies for increasing the reactor efficiency encompass adding multiple components or additional steps (for example to incorporate heat recovery [4], [5]), which are detrimental to the power output and power density (as they are inversely proportional to the cycle duration and system volume). In Figure 1 we present the theoretical power density for  ${\rm CeO_2}$ -based system as a function of the difference in nonstoichiometry between reduction and oxidation  $\Delta\delta$  and the cycle duration  $t_{\rm cycle}$ , assuming 50% porosity and considering only the volume of the redox-active material (upper bound case).

The figure also includes the calculated power density for two experimental demonstrations: the 50 kW<sub>th</sub> input volumetric solar receiver reactor by Zoller et al. [1] (with 5.6% reactor efficiency for  $CO_2$  splitting), and the 4.4 kW<sub>th</sub> input packed bed reactor by Hathway et al. [3] (0.72% reactor efficiency for  $CO_2$  splitting). It shows that while Hathway's isothermal packed bed reactor had lower reactor efficiency, it was able to demonstrate power density which is at its theoretical limit and an order of magnitude higher than that of the volumetric reactor. Another aspect that is often overlooked is the additional energy required for the product separation due to the low conversion extent; both demonstrations had low conversion extent, which means that an energy/CAPEX-intensive separation process is required between the redox reactor and any GTL unit. In the case of  $CO/CO_2$  separation, the cost for such a unit, especially under low conversion, can cost more than the chemical reactor [6].

# 2. System Description

With these points in mind, we have developed a new reactor concept based on a packed-bed design, that could achieve high conversion extents under operating conditions comparable to the state-of-the-art. The design utilizes the continuous chemical potential of nonstoichiometric oxides such as ceria-based oxides, ferrites, and perovskites, achieving similar performance to that of countercurrent systems without the complexity and limitations of high-temperature membranes or moving oxide systems, by storing the chemical potential in a packed bed of oxide material [7], [8]. The operating principle is presented in Figure 2. This design also allows to decouple the reactor from the solar receiver and enables the possibility of a hybrid CST-electrical heating system, benefiting from the superior performance of each method at different temperatures. A higher capacity factor than directly irradiated reactors can be obtained using a thermal energy storage (TES) system. Considering that CST systems are deployed in areas with high solar resources, there is also a great potential synergy with PV-based heating. We compare the cases of using CST only for providing both heat and power against the hybrid CST-PV configuration, in which process heat is provided by CST and power is provided by PV.

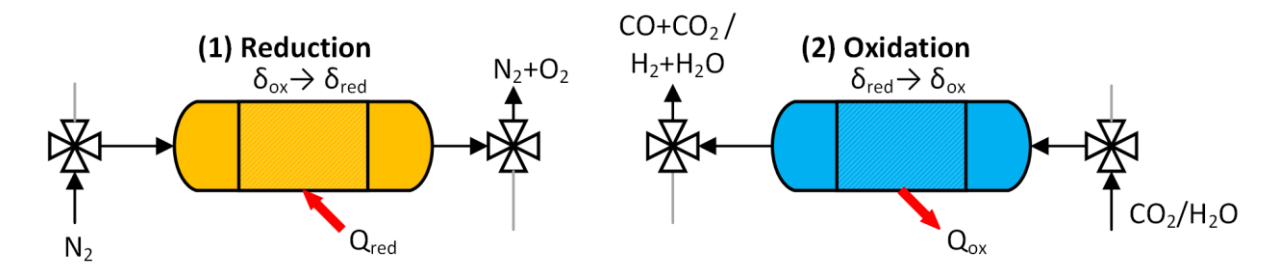
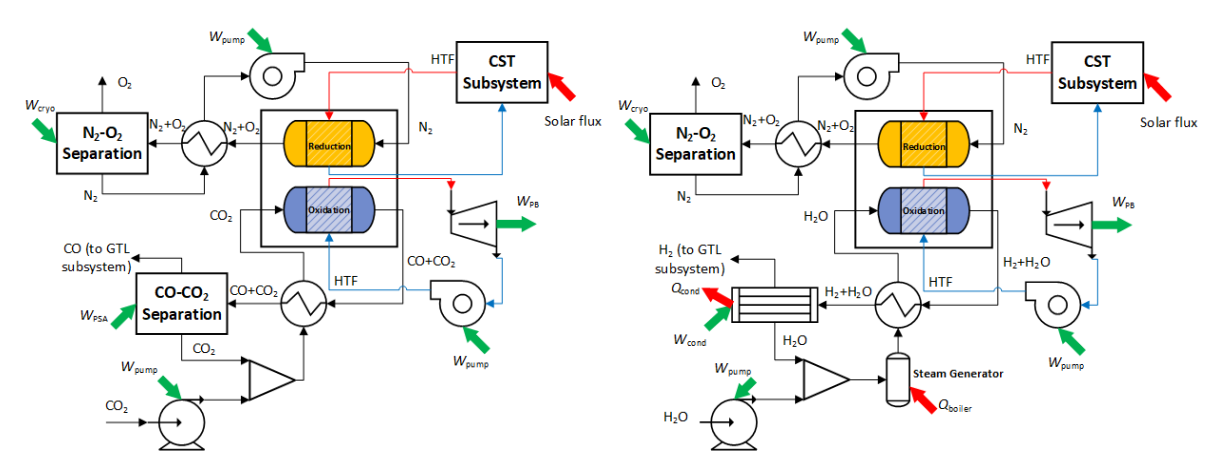


Figure 2. The operational scheme of the redox reactors

In this preliminary study we evaluate the technoeconomic performance of the system without any storage, directly using the collected CST heat to drive the plant. The system is modular, consisting of multiple stacks of reactors that allow continuous syngas production at a given rate and composition, by making sure that at each given time, the same number of reactors are undergoing oxidation. This design can also benefit from separating the CO<sub>2</sub> and H<sub>2</sub>O splitting, since each subsystem requires different auxiliary units. These can be centralized and

sized to meet the equivalent steady-state production capacity and serve all reactor stacks. The process flow diagrams of the CO<sub>2</sub> and H<sub>2</sub>O subsystems are presented in Figure 3.



**Figure 3.** Process flow diagrams of the plant. Left: CO<sub>2</sub> splitting subsystem. Right: H<sub>2</sub>O splitting subsystem. Each stack consists of multiple reactors (only two are depicted for simplicity).

In this work we model the GTL subsystem as a model Fischer-Tropsch reaction, assuming full conversion. The CST subsystem is a central tower receiver that delivers high-temperature heat using a heat transfer fluid (HTF). CST tower receivers operating at temperatures required for the CeO<sub>2</sub> reduction reaction are under development but not currently commercially available and, as such, the receiver technology is not considered in detail in this analysis. A Brayton power cycle utilizes the exothermic oxidation heat, to produce power via an HTF loop during the oxidation step.

# 3. Model Description

The regenerative countercurrent packed bed redox reactors are modeled as a 1D domain, assuming the radial distribution is uniform. The convection-diffusion equation is solved for all participating species ( $O_2$  for reduction,  $O_2$ ,  $CO_2$ , and CO for oxidation with  $CO_2$ , and  $O_2$ ,  $H_2O$ , and  $H_2$  for oxidation with  $H_2O$ ):

$$\varepsilon \frac{\partial c_{A}}{\partial t} = D_{\text{eff}} \frac{\partial^{2} c_{A}}{\partial x^{2}} + u_{A} \frac{\partial c_{A}}{\partial x} + v_{A} C_{\text{CeO}_{2}} \frac{\partial \delta}{\partial t}$$
(4)

with  $\varepsilon$  as the void fraction,  $\mathcal{C}_A$  as the concentration of species A,  $\mathcal{D}_{eff}$  as the effective diffusion coefficient,  $u_A$  as the fluid flow velocity,  $v_A$  as the stoichiometric coefficient (from Eq. (1)-(3)), and  $\mathcal{C}_{CeO_2}$  as the ceria concentration. The velocity  $u_A$  is taken as a positive or negative value for the oxidation and reduction steps respectively. The source term is modeled per [8] as

$$\frac{d\delta}{dt} = k_0 \left( \delta_{\text{eq}} (T_{\text{red}}, C_{\text{O}_2}) - \delta \right) \Theta \left( \delta_{\text{eq}} (T_{\text{red}}, C_{\text{O}_2}) - \delta \right)$$
 (5)

for the reduction step and

$$\frac{d\delta}{dt} = -k_0 \left( \delta - \delta_{\text{eq}} (T_{\text{ox}}, C_{\text{O}_2}) \right) \Theta \left( \delta - \delta_{\text{eq}} (T_{\text{ox}}, C_{\text{O}_2}) \right)$$
 (6)

for the oxidation step.  $k_0$  is the rate constant,  $\delta$  is the local non-stoichiometry, and  $\delta_{\rm eq}$  is the local equilibrium non-stoichiometry with the gas phase.  $\Theta$  is a Heaviside function designed to prevent the source term from going over equilibrium, and  $\delta_{\rm eq}$  is calculated from [9].

The unit operations presented in Figure 3 are analyzed using thermodynamics calculations, with the baseline parameters per Table 1. A solar field is designed using SolarPILOT, with the receiver thermal losses modeled as:

$$q_{\text{rec,loss}} = \varepsilon \sigma (T_{\text{rec}}^4 - T_0^4) + h(T_{\text{rec}} - T_0)$$
(7)

The analysis includes tower piping losses, and the receiver temperature is higher than the reduction temperature to allow for a driving force for the endothermic reduction reaction  $T_{\rm rec} = T_{\rm red} + 100$ . Additionally, we also model the system assuming an advanced high-temperature receiver technology that can minimize the thermal losses such as in [10]. We assume that the system can operate under partial load due to the modularity (multiple reactors/stacks) as well as under flexible operating conditions by controlling the flow rates and/or step duration, which has been verified using the 1D reactor model. For the CST-PV case without interconversion between heat and electricity, the hourly capacity factor f equals the lower of the two capacity factors, thermal  $f_{\rm th}$  and electrical  $f_{\rm el}$ . An alternative design, adding electrical heaters to convert excess PV electricity to heat when  $f_{\rm elec} > f_{\rm th}$  and oversizing the power block to allow conversion of excess heat to electricity when  $f_{\rm th} > f_{\rm elec}$  is also considered. The PV nameplate capacity is set to meet the design point power requirements. For the solar resources analysis, the plant is located in Daggett, CA using typical meteorological year (TMY) weather data.

Table 1. Parameters for the base case system and TEA model

	Parameter	Value	Unit	Ref.
Reactor	Reactor length, L	1	m	
	Reactor diameter, d	0.3	m	
	Packed bed void fraction, $\varepsilon$	0.5		
	Redox material	CeO <sub>2</sub>		
Reduction	Reduction temperature, $T_{\rm red}$	1500	°C	
	Reduction pressure, $p_{ m red}$	1	bar	
	Sweep gas flowrate, $\dot{n}_{ m sg}$	0.5	mol s <sup>-1</sup>	
	Sweep gas purity, $x_{O_2,in}$	$10^{-5}$		
	Reduction time, $t_{\rm red}$	150	S	
	Solid heat recovery effectiveness, $\varepsilon_{ m HR}$	0.5		[2], [4]
Oxidation	Oxidation temperature, $T_{ox}$	950	°C	
	Oxidation pressure, $p_{ox}$	1	bar	
	Oxidizer flowrate, $\dot{n}_{ m ox}$	0.1	mol s <sup>-1</sup>	
	Oxidation time, $t_{ox}$	$t(X=0.5X_{\rm eq})$	S	
	Exothermic heat recovery eff., $\varepsilon_{\mathrm{ex}}$	0.8		
Gas-to-liquid	Fischer-Tropsch temperature, $T_{\rm FT}$	200	°C	[11]
	Fischer-Tropsch pressure, $p_{ m FT}$	10	bar	[11]
	Fischer-Tropsch conversion, $X_{\rm FT}$	1		
	Syngas composition H₂:CO	2:1		
CST	Receiver design point power, $P_{\text{rec}}$	20	MW	
	Design point field efficiency, $\eta_{ m field}$	0.497		
	Receiver thermal efficiency, $\eta_{ m rec}$	0.621		
Auxiliary	PSA efficiency (CO <sub>2</sub> -CO), $\eta_{PSA}$	0.05		[12]
	PSA pressure, $p_{PSA}$	8	bar	
	Power block cycle efficiency, $\eta_{\mathrm{PB}}$	0.535		[13]
	Pump/compressor efficiency, $\eta_{ m pump}$	0.85		
	Cryogenic air separation energy, $w_{ m sep}$	15	$kJ mol_{N_2}^{-1}$	[14]
Financial	Fixed charge rate, FCR	7.07	%	[15]
	Total as-spent cost to total overnight cost, TASC/TOC	1.093		[15]

The economic and financial parameters for the PV and CST subsystems have been taken from NREL's ATB with adjustments (2035 advanced scenario, CST excludes the power block as it is accounted for separately) using SAM's financial models, with a receiver cost of 100

\$/kW and heliostat cost of \$50/m² (DOE SETO SunShot 2030 targets). The CAPEX of the redox reactors has been estimated from data for catalytic reformers [16] but adding the cost for the redox material on top (while keeping the original catalyst costs, used as a multiplier for more expensive materials needed due to the higher operating temperature than conventional reformers). The power block cost is taken from [13]. The levelized cost of product (fuel) is then calculated from [17]:

$$LCOP = \frac{FCR \cdot TCC + FOC - REV}{m_{\text{fuel}}} + VOC + LCOE_{PV} \frac{P_{PV}}{m_{\text{fuel}}} + LCOH_{CST} \frac{P_{CST}}{m_{\text{fuel}}}$$
(8)

with the total capital cost TCC equals to the total as-spent capital cost (TASC), FOC as the fixed operating costs, REV the revenue from selling industrial grade  $O_2$ ,  $m_{\rm fuel}$  as the annual fuel production, VOC as the variable operating costs, and the PV and CST levelized costs of heat  ${\rm LCOE_{PV}}$  and  ${\rm LCOH_{CST}}$ , multiplied by the ratio of the respective power needed per mass unit of fuel  $\frac{P_{\rm PV}}{m_{\rm fuel}}$  and  $\frac{P_{\rm CST}}{m_{\rm fuel}}$ . Both the  ${\rm LCOE_{PV}}$  and  ${\rm LCOH_{CST}}$  are calculated in the same manner using the FCR method and their respective financial input data. The FCR method includes the recovery period of the plant, taken as 30 years in accordance with NETL guidelines for TEA of energy systems [15].

#### 4. Results and Discussion

Using our model for the baseline case Table 1 resulted in an LCOP of \$189.23/gal for the hybrid CST-PV without energy conversion between CST and PV, \$175.82/gal for the hybrid CST-PV with energy conversion, and \$623.05/gal for the CST only case. These numbers are two orders of magnitude larger than the selling price of jet fuel, and are not close to any commercial viability even with tax incentives. The main identified factors are the low conversion extents (9.8% for CO<sub>2</sub> and 5.2% for H<sub>2</sub>O) and power densities (<3 kW m<sup>3</sup>), which in turn increase the CAPEX of the separation units while lowering the overall plant fuel output capacity.

To identify more promising configurations, we have performed a parametric study, in which we examined the following: (a) increasing  $T_{\rm red}$  to 1600°C; (b) lowering  $T_{\rm ox}$  to 700°C, identified from analysis of the redox reactors as the optimal temperature for  $T_{\rm red}=1600$ °C; (c) varying the CST subsystem in the range of 10-30 MW; (d) assuming an advanced receiver with  $\eta_{\rm rec}=0.9$ ; and (e) changing the number of reactors in a stack and number of stacks (to identify more efficient designs). When varying the receiver design point power, the chemical process and rest of the plant, including PV, are scaled accordingly to accommodate the larger thermal power available.

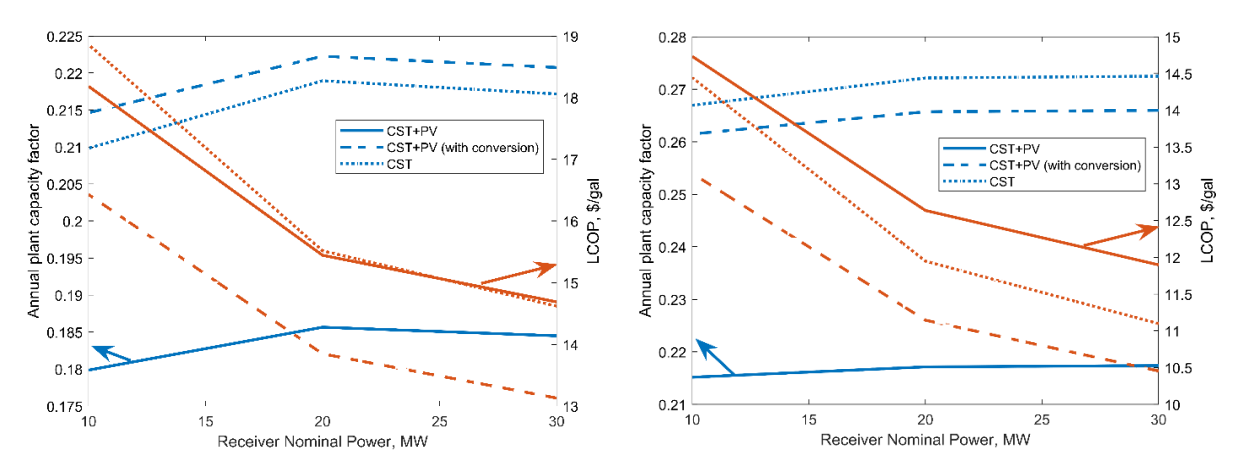


**Figure 4.** The annual plant capacity factor and levelized cost of product (fuel) vs. the receiver nominal power. Left: receiver with thermal losses per eq. (7). Right: advanced receiver with  $\eta_{rec} = 0.9$ . All cases are for  $T_{red} = 1600$ °C,  $T_{ox} = 700$ °C while the other inputs are per the base case.

The effect of varying the receiver nominal power is presented in Figure 4 for the normal receiver (thermal losses calculated per eq. (7)) and the advanced receiver (fixed thermal efficiency  $\eta_{\rm rec}=0.9$ ). For each receiver power value, we present the results for the hybrid CST+PV, hybrid CST+PV with energy conversion, and CST cases. The suggested improvements drastically reduce the cost of the fuel by an order of magnitude, reaching a value of \$10.45/gal for the case of advanced receiver at 30 MW design power and for the CST+PV case with energy conversion. Larger plant sizes exhibit lower LCOP due to improved economy of scale. For the advanced receiver design, it seems that the PV field size is constraining the capacity factor. From a price perspective, the hybrid CST+PV case with energy conversion is able to be the most competitive. To assess the effects of heat recovery on the cost, we have varied the value of the solid heat recovery effectiveness  $\varepsilon_{\rm HR}$  from 0 to 1 (although a value of 1 is not feasible, we included it to estimate the theoretical limit). The results are depicted in Figure 5.

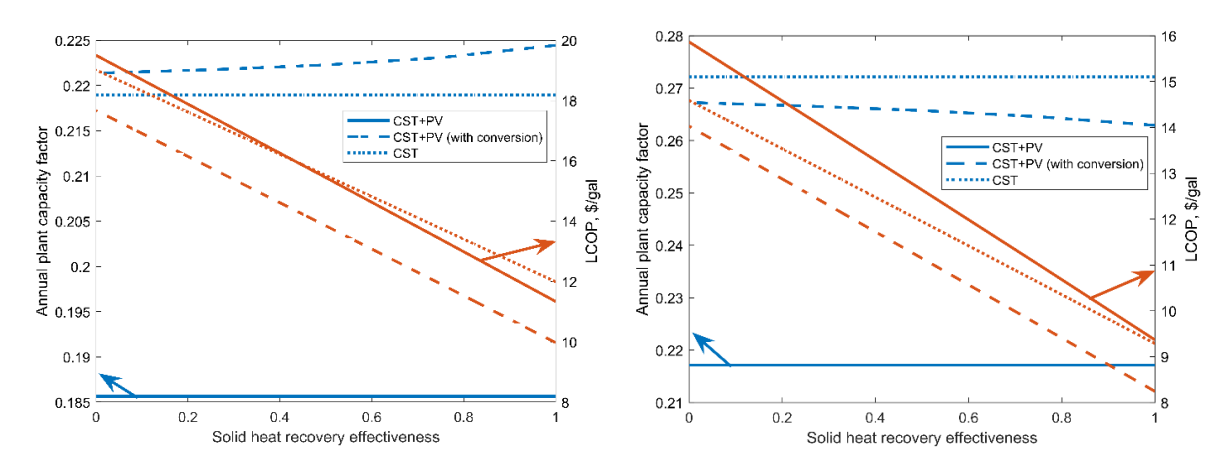


**Figure 5.** The annual plant capacity factor and levelized cost of product (fuel) vs. the solid heat recovery effectiveness. Left: receiver with thermal losses per eq. (7). Right: advanced receiver with  $\eta_{rec} = 0.9$ . Results for  $T_{red} = 1600^{\circ}C$ ,  $T_{ox} = 700^{\circ}C$ ,  $T_{rec} = 30$  MW (other input is per the base case).

Increasing heat recovery lowers LCOP due to lowering the high-temperature heat requirement, but capacity factors are not significantly affected. It is also important to note that such a plant has an annual capacity of 100-1000s tons of jet fuel per year, putting it in a demo plant scale. Since a single high-flux high-temperature receiver at much larger scales will suffer from low field efficiency, any commercial deployment would need to employ multiple towers to reach a commercial scale production capacity. Some cost improvements are feasible since central units such as syngas conditioning and GTL plant operation units will benefit from the economy of scale. However, siting requirements might pose additional geographical limitations. An alternative H<sub>2</sub>-H<sub>2</sub>O separation method, using mechanical vapor recompression cycle [18], can also improve the overall system energy efficiency and potentially reduce the costs.

### 5. Conclusions

A preliminary TEA framework for a solar fuels plant has been developed, using physics-based correlations in lieu of the simpler figure-of-merit approach which is usually favored. This allows us to elucidate the connections between technical parameters, such as reduction temperature, and the financial performance metrics. CST-PV hybrid system with energy conversion is identified as the most promising among the cases studied. While the preliminary cost predictions are significantly higher than current aviation fuel prices (~\$2.2/gal), there is still a large parameter space that can be explored to identify optimal operating conditions and plant scale. In addition, a full cost sensitivity analysis needs to be performed to identify the major cost drivers, thus helping direct future work into the most impactful areas. The optimization of the CST and PV systems could potentially improve the performance of the hybrid case. Lastly, the inclusion

of a TES unit should be explored, as it can drastically increase the capacity factor and annual production output.

## Data availability statement

The data supporting this analysis can be made available upon a reasonable request.

## **Author contributions**

**Alon Lidor:** Conceptualization, Methodology, Analysis, Writing – Original Draft. **Zachary Hart:** Methodology, Analysis, Writing – Review & Editing. **Janna Martinek:** Methodology, Analysis, Writing – Review & Editing.

## **Competing interests**

The authors declare that they have no competing interests.

## **Funding**

The material is based upon work supported by U.S. Department of Energy, Office of Science, Office of Workforce Development for Teachers and Scientists (WDTS) under the Science Undergraduate Laboratory Internship (SULI) program.

# **Acknowledgement**

This work was authored in part by the National Renewable Energy Laboratory, operated by Alliance for Sustainable Energy, LLC, for the U. S. Department of Energy (DOE) under Contract No. DE-AC36-08GO28308. The views expressed in the article do not necessarily represent the views of the DOE or the U.S. Government. The U.S. Government retains and the publisher, by accepting the article for publication, acknowledges that the U.S. Government retains a nonexclusive, paid-up, irrevocable, worldwide license to publish or reproduce the published form of this work, or allow others to do so, for U.S. Government purposes.

#### References

- [1] S. Zoller *et al.*, "A solar tower fuel plant for the thermochemical production of kerosene from H<sub>2</sub>O and CO<sub>2</sub>," *Joule*, vol. 6, no. 7, pp. 1606–1616, Jul. 2022, doi: 10.1016/j.joule.2022.06.012.
- [2] A. Lidor and B. Bulfin, "A critical perspective and analysis of two-step thermochemical fuel production cycles," *Solar Compass*, p. 100077, Jun. 2024, doi: 10.1016/j.sol-com.2024.100077.
- [3] B. J. Hathaway, R. Bala Chandran, A. C. Gladen, T. R. Chase, and J. H. Davidson, "Demonstration of a Solar Reactor for Carbon Dioxide Splitting via the Isothermal Ceria Redox Cycle and Practical Implications," *Energy & Fuels*, vol. 30, no. 8, pp. 6654–6661, Aug. 2016, doi: 10.1021/acs.energyfuels.6b01265.
- [4] A. Lidor, Y. Aschwanden, J. Häseli, P. Reckinger, P. Haueter, and A. Steinfeld, "High-temperature heat recovery from a solar reactor for the thermochemical redox splitting of H<sub>2</sub>O and CO<sub>2</sub>," *Applied Energy*, vol. 329, p. 120211, Jan. 2023, doi: 10.1016/j.apen-ergy.2022.120211.
- [5] A. Lidor and L. Zimmermann, "Experimental demonstration of high-temperature heat recovery in a solar reactor," *Solar Energy*, vol. 262, p. 111915, Sep. 2023, doi: 10.1016/j.solener.2023.111915.

- [6] G. Zang, P. Sun, A. A. Elgowainy, A. Bafana, and M. Wang, "Performance and cost analysis of liquid fuel production from H<sub>2</sub> and CO<sub>2</sub> based on the Fischer-Tropsch process," *Journal of CO2 Utilization*, vol. 46, p. 101459, Apr. 2021, doi: 10.1016/j.jcou.2021.101459.
- [7] I. S. Metcalfe *et al.*, "Overcoming chemical equilibrium limitations using a thermodynamically reversible chemical reactor," *Nature Chemistry*, vol. 11, no. 7, pp. 638–643, 2019, doi: 10.1038/s41557-019-0273-2.
- [8] B. Bulfin, M. Zuber, O. Gräub, and A. Steinfeld, "Intensification of the reverse water–gas shift process using a countercurrent chemical looping regenerative reactor," *Chemical Engineering Journal*, vol. 461, Apr. 2023, doi: 10.1016/j.cej.2023.141896.
- [9] B. Bulfin *et al.*, "Statistical thermodynamics of non-stoichiometric ceria and ceria zirconia solid solutions," *Physical Chemistry Chemical Physics*, vol. 18, no. 33, pp. 23147–23154, 2016, doi: 10.1039/C6CP03158G.
- [10] G. Ambrosetti and P. Good, "A novel approach to high temperature solar receivers with an absorbing gas as heat transfer fluid and reduced radiative losses," *Solar Energy*, vol. 183, no. February, pp. 521–531, 2019, doi: 10.1016/j.solener.2019.03.004.
- [11] A. de Klerk, Fischer-Tropsch Refining. Wiley, 2011. doi: 10.1002/9783527635603.
- [12] K. Z. House, A. C. Baclig, M. Ranjan, E. A. van Nierop, J. Wilcox, and H. J. Herzog, "Economic and energetic analysis of capturing CO2 from ambient air," *Proceedings of the National Academy of Sciences*, vol. 108, no. 51, pp. 20428–20433, Dec. 2011, doi: 10.1073/pnas.1012253108.
- [13] B. T. Gorman, M. Lanzarini-Lopes, N. G. Johnson, J. E. Miller, and E. B. Stechel, "Techno-Economic Analysis of a Concentrating Solar Power Plant Using Redox-Active Metal Oxides as Heat Transfer Fluid and Storage Media," *Front. Energy Res.*, vol. 9, Dec. 2021, doi: 10.3389/fenrg.2021.734288.
- [14] H. W. Häring, *Industrial Gases Processing*. Wiley-VCH, 2008. doi: 10.1002/9783527621248.
- [15] J. Theis, "Quality Guidelines for Energy Systems Studies: Cost Estimation Methodology for NETL Assessments of Power Plant Performance," National Energy Technology Laboratory (NETL), Pittsburgh, PA, Morgantown, WV, and Albany, OR (United States), NETL-PUB-22580, Feb. 2021. doi: 10.2172/1567736.
- [16] E. Lewis et al., "Comparison of Commercial, State-of-the-Art, Fossil-Based Hydrogen Production Technologies," National Energy Technology Laboratory (NETL), Pittsburgh, PA, Morgantown, WV, and Albany, OR (United States), DOE/NETL-2022/3241, Apr. 2022. doi: 10.2172/1862910.
- [17] J. A. Martin, E. C. D. Tan, D. A. Ruddy, J. King, and A. T. To, "Temperature—Pressure Swing Process for Reactive Carbon Capture and Conversion to Methanol: Techno-Economic Analysis and Life Cycle Assessment," *Environ. Sci. Technol.*, vol. 58, no. 31, pp. 13737–13747, Aug. 2024, doi: 10.1021/acs.est.4c02589.
- [18] A. Lidor, "Hydrogen-steam separation using mechanical vapor recompression cycle," *International Journal of Hydrogen Energy*, vol. 94, pp. 664–668, Dec. 2024, doi: 10.1016/j.ijhydene.2024.11.040.